Asian Journal of Chemistry; Vol. 27, No. 11 (2015), 4071-4075

ASIAN JOURNAL OF CHEMISTRY

http://dx.doi.org/10.14233/ajchem.2015.19090

Environmental Remediation of Pb(II) Solutions by Photocatalytic Reduction Using S-CeO_2 Nanocomposite

E.S. BAEISSA

Chemistry Department, Faculty of Science, King Abdulaziz University, P.O. Box 80203, Jeddah 21589, Saudi Arabia

Corresponding author: Fax: +966 2 6952292; Tel: +966 6400000; E-mail: elhambaeissa@yahoo.com

Received: 9 February 2015; *Accepted*: 18 March 2015; *Published online*: 16 July 2015; AJC-17405

A sol-gel method was used to prepare CeO_2 and S-CeO_2 nanocomposite. CeO_2 and S-CeO_2 nanocomposites were characterized by BET, XRD, XPS, photoluminescence, UV-visible and TEM measurements. The photocatalytic performance of CeO_2 and S-CeO_2 nanocomposites with respect to the photocatalytic reduction of lead under visible light irradiation was determined. The results reveal that the sulfur was well dispersed onto the surface of the ceria nanoparticles. Additionally, the surface area of the S-CeO_2 nanocomposites was observed to be smaller than that of the CeO_2 nanoparticles due to the blocking of some pores of the CeO_2 nanoparticles by the doping of sulfur. The S-CeO_2 nanocomposite (1.5 wt % as sulfur) exhibits the lowest band gap and highest photocatalytic activity for reduction of lead. The photocatalytic performance of the 1.5 wt % S-CeO_2 nanocomposites was stable after the reuse of the nanoparticles for reduction of lead after five uses.

Keywords: CeO_2, S doping, Photocatalyst, Lead reduction.

INTRODUCTION

Some benefits to human beings come from the industrialization, but the industrialization cause problems to the environment. One of them is water pollution, several industries cause water pollutions. Pollutions by heavy metals is a one of the most dangerous problem and very difficult to treat. Lead in water even at small levels is very dangerous, the Agency for Toxic Substances and Disease Registry classified lead as the second top water hazard that requires urgent removal[1]. Either the industrialization harmful by-products or the nature throughout acid rock drainage and the anthropogenic activities such as household plumping regard as source of contamination of water by lead. Many problems can be caused to human health such as brain damage due to prolong exposure to lead. According to the Environmental Protection agency, 15 ppb is the maximum safe level of lead in drinking water, according to the World Health Organization, 10 ppb is the maximum safe level of lead in drinking water[2,3]. Many methods were used to removal of lead from water[4,5], but the disadvantage of these methods are produce of harmful by-products[6], need pretreatment[7], need long residence time[8] and very expansive[9]. By using photocatalysis process, we can overcome these limitations. Titanium dioxide regard as the most active photocatalyst due to its stability and activity. The absorption of titanium dioxide is limited to UV region is one of the limitations of this process. We can overcome this limitation by metal doping such as tungsten[10-13]. Doping of titanium dioxide by metal lead to shift absorption from UV to visible region. Another method is coupling of titanium dioxide by semiconductor oxide such as WO_3[14-16]. Cerium dioxide can be used in many applications such as ultraviolet blocking materials, gates for metaloxide semiconductor devices and phosphors, oxygen gas sensors, fluorescent materials, acting as the three-way catalysts in vehicle emission control systems, *etc*.[17-20]. Now days, cerium dioxide was prepared by different methods to control sizes and morphologies[21-26]. Cerium dioxide was used as a photocatalyst for degradation of methylene blue dye under UV light[27]. So it still remain a great aim to convert the absorption of ceria from UV to visible region. The present study presents the synthesis and characterization of S-CeO_2 and the evaluation of its photocatalytic activity for the reduction of lead in the aqueous phase.

EXPERIMENTAL

Preparation of photocatalyst: All chemicals used in this study were used as received without any further purification. Initially, CeO_2 was prepared by the following method: 3.0 g of dodecylamine dissolve in 30 g of water, 0.04 g of 36 % HCl dissolve in 10 g of water, then HCl solution added dropwise to dodecylamine solution and the resulting solution (A) was

stirred for 1 h, 0.8 g of cerium isopropoxide dissolved in 18 g of isopropyl alcohol and the resulting solution (B) was stirred for 1 h. Adding solution A to solution B and the resulting solution was stirred for 24 h followed by filtration and calcination for 5 h at 550 °C. S-CeO_2 (containing 0.5, 1.0, 1.5 and 2.0 wt % of S) was synthesized using the same method for preparation of CeO_2, except in case of S-CeO_2, we mix cerium isopropoxide was thiourea as source for sulfur.

Characterization techniques: X-ray diffraction (XRD) analysis was performed at room temperature with a Bruker axis D8 using Cu-K_α radiation (λ = 1.540 Å). The specific surface area was calculated from N_2-adsorption measurements, which were obtained using a Nova 2000 series Chromatech apparatus at 77 K. Prior to the measurements, the samples were treated under vacuum at 100 °C for 2 h. The band gap of the samples was identified by UV-visible diffuse reflectance spectroscopy (UV-Vis-DRS), which was performed in air at room temperature over the wavelength range of 200-800 nm using a UV/Vis/NIR spectrophotometer (V-570, JASCO, Japan). Transmission electron microscope (TEM) analysis was conducted with a JEOL-JEM-1230 microscope and samples were prepared by suspension in ethanol, followed by ultrasonication for 30 min. Subsequently, a small amount of this solution was placed onto a carbon-coated copper grid and dried before loading the sample into the TEM. X-ray photoelectron spectroscopy (XPS) studies were performed using a Thermo Scientific K-ALPHA, XPS, England. Photoluminescence emission spectra were recorded using a Shimadzu RF-5301 fluorescence spectrophotometer.

Photocatalysis experiment: The application of synthesized nanocomposite for the photodegradation of cyanide was investigated under visible light. The experiments were carried out using a horizontal cylinder annular batch reactor. The photocatalyst was irradiated with a blue fluorescent lamp (150 W) and the reactor doubly covered with a UV cut filter. In a typical experiment, weight of catalyst were suspended into a 300 mL, 100 mg/L lead nitrate solution. The reaction was carried out isothermally at 25 °C and samples of the reaction mixture were taken at different intervals for a total reaction time of 1 h. The lead concentration in the samples was estimated by atomic absorption. The adsorption efficiency of Pb has been measured by applying the following equation:

$$\text{Adsorption efficiency of Pb}\,(\%) = \frac{(C_o - C)}{C_o} \times 100$$

where C_o is the initial concentration of lead in solution, C is the remaining concentration of lead in solution.

RESULTS AND DISCUSSION

Structural, morphological and compositional characterizations: Fig. 1 shows the XRD patterns of the CeO_2 and S-CeO_2 nanocomposites. The results reveal that the nanocomposites are mainly composed of CeO_2, which indicates that the lack of diffraction peaks due to S or SO_2 in the patterns of the S-CeO_2 samples is because the wt % of S is below the XRD detection limit or perhaps because S is well dispersed on surface of the CeO_2 nanoparticles.

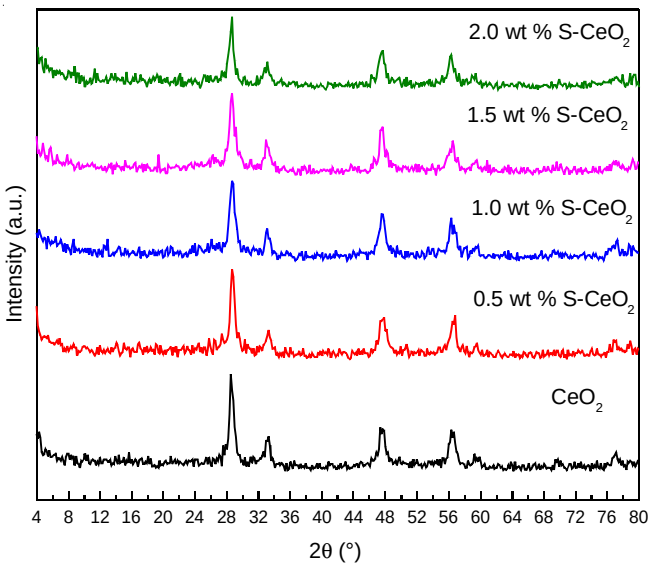

Fig. 1. XRD patterns of CeO_2 and S-CeO_2 nanocomposites

Fig. 2 shows the XPS spectra of S2p for a sample of S-CeO_2. The results reveal the presence of S in the sample *via* the peak for S 2p at 169.2 eV.

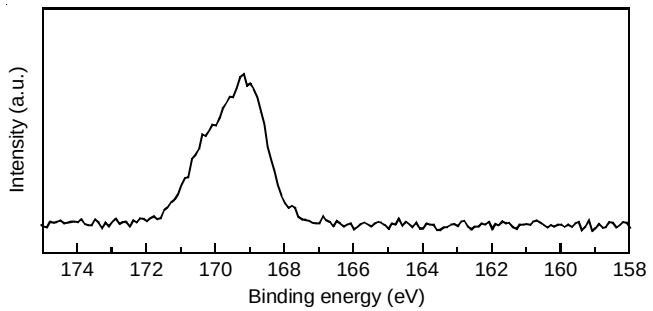

Fig. 2. XPS spectra of S 2p for the 1.5 wt % S-CeO_2 sample

Fig. 3 shows TEM images of CeO_2 and 1.5 wt % S-CeO_2 nanocomposites. The results show that shape of CeO_2 is a spherical and sulfur is dispersed well on the surface of CeO_2.

Surface area analysis: The texture parameters of the CeO_2 and S-CeO_2 nanocomposites are presented in Table-1. The S_{BET} values for CeO_2 and 0.5 wt % S-CeO_2, 1.0 wt % S-CeO_2, 1.5 wt % S-CeO_2 and 2.0 wt % S-CeO_2 were determined to be 70, 67, 65, 63 and 58 m^2/g, respectively. The total pore volume of S-CeO_2 is smaller than that of the CeO_2 sample due to the blocking of some pores by deposition of sulfur. The presence of mesopores in all samples was confirmed by the similar values of S_{BET} and S_t in most samples, as presented in Table-1.

Optical characterization: Fig. 4 shows the UV-visible diffuse reflectance spectra of the CeO_2 and S-CeO_2 nanocomposites. The results demonstrate that the doping of sulfur onto the surface of CeO_2 leads to a shift in the absorption edge of CeO_2 from 350 nm to 450 nm. The UV-visible spectra were used to calculate the direct band gap of the CeO_2 and S-CeO_2 nanocomposites based on a method used by Mohamed and Mkhalid[28]. The band gap energies were calculated using the following equation:

$$E_g = 1239.8/\lambda$$

TABLE-1
TEXTURE PARAMETERS OF CeO_2 AND S-CeO_2 NANOCOMPOSITES

Sample	S_{BET} (m^2/g)	S_t (m^2/g)	S_{micro} (cm^2/g)	S_{ext} (cm^2/g)	V_p (cm^3/g)	V_{micro} (cm^3/g)	V_{meso} (cm^3/g)	r (Å)
CeO_2	70.00	71.00	44.00	26.00	0.250	0.180	0.070	30.00
0.1 wt % S-CeO_2	67.00	67.00	43.00	24.00	0.195	0.150	0.045	40.00
0.2 wt % S-CeO_2	65.00	65.00	42.00	23.00	0.172	0.130	0.042	50.00
0.3 wt % S-CeO_2	63.00	63.00	41.00	22.00	0.165	0.125	0.040	55.00
0.4 wt % S-CeO_2	58.00	59.00	39.00	19.00	0.150	0.115	0.030	60.00

Note: S_{BET} = BET-surface area; S_t = Surface area derived from V_{l-t} plots; S_{mic} = Surface area of micropores; S_{ext} = External surface area; V_p = Total pore volume; V_{micro} = Volume of micropores; V_{meso} = Volume of mesopores; r = Mean pore radius.

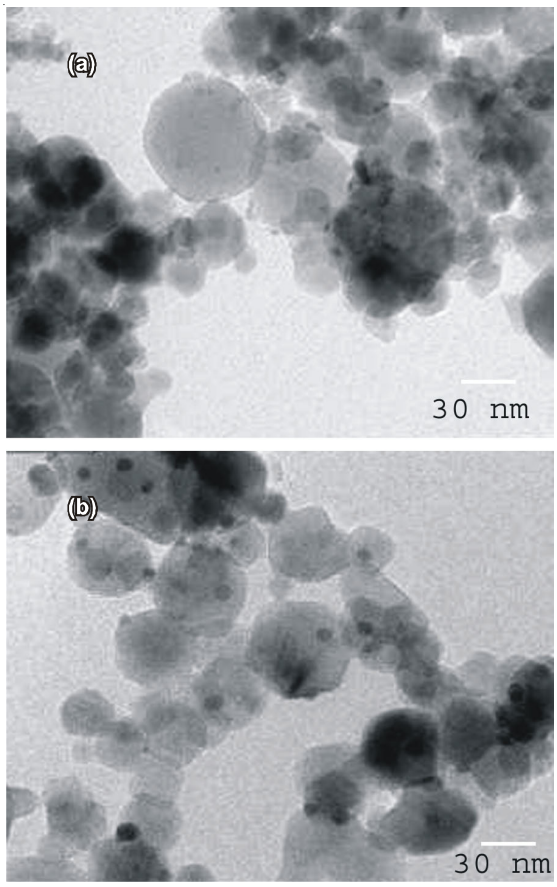

Fig. 3. TEM images of CeO_2 (A) and 1.5 wt % S-CeO_2 (B) nanocomposites

where E_g is the band gap (eV) and λ is the wavelength (nm) of the absorption edges in the spectrum (Table-2). The results reveal that an increase in the wt % of sulfur from 0.0 to 1.5 wt % decreases the band gap from 3.54 to 2.82 eV. However, there is no significant effect on the band gap at a high wt % of sulfur greater than 1.5. Therefore, there is an optimum content of deposited sulfur that controls the band gap.

TABLE-2
BAND GAP ENERGY OF CeO_2 AND S-CeO_2 NANOCOMPOSITES

Sample	Band gap energy (eV)
CeO_2	3.54
0.5 wt % S-CeO_2	3.33
1.0 wt % S-CeO_2	3.01
1.5 wt % S-CeO_2	2.82
2.0 wt % S-CeO_2	2.78

We investigated the separation and recombination of photogenerated charge carriers and the transfer of the photogenerated electrons and holes by gathering photoluminescence emission spectra. Fig. 5 shows photoluminescence spectra of CeO_2 and S-CeO_2 nanocomposites. The results indicate that an increase in the wt % of sulfur doped on the CeO_2 nanoparticles from 0.0 wt % to 1.5 wt % leads to a decrease in the photoluminescence intensity. However, there is no significant effect on the photoluminescence intensity at a high wt % of sulfur above 1.5. Therefore, there is an optimum content of deposited sulfur that yields the carrier lifetime required for e-h recombination, in agreement with the UV-visible results.

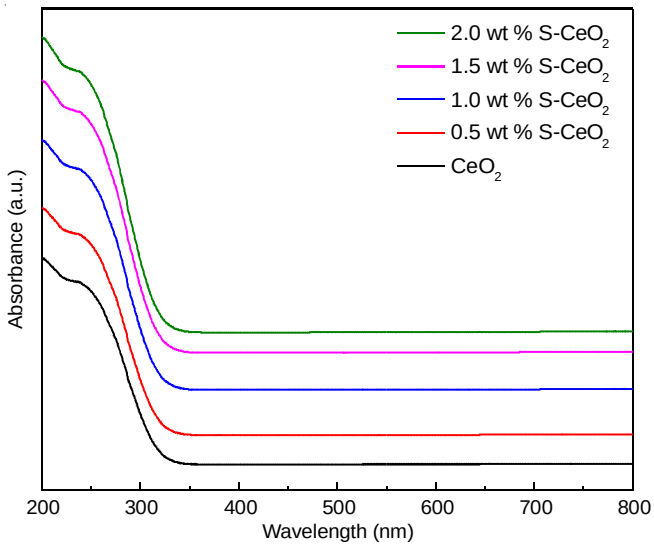

Fig. 4. UV-visible absorption spectra of CeO_2 and S-CeO_2 nanocomposites

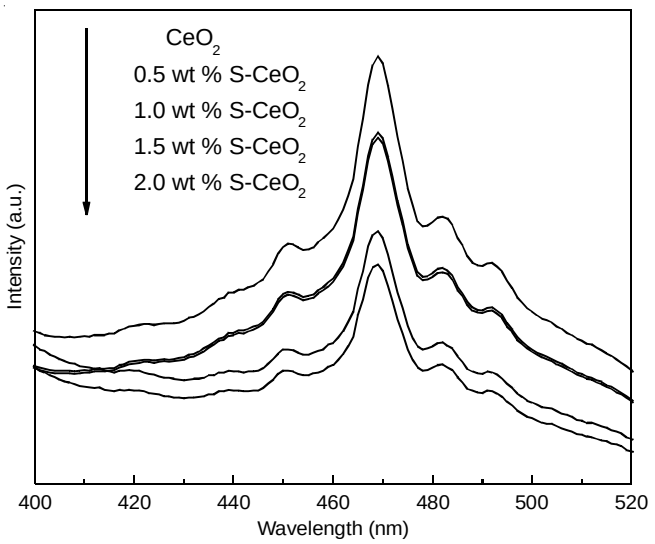

Fig. 5. Photoluminescence spectra of CeO_2 and S-CeO_2 nanocomposites

Photocatalytic activities: Fig. 6 shows the effect of the wt % of sulfur on the photocatalytic activity of CeO_2 nanoparticles for photocatalytic reduction of lead under visible light irradiation. The experiment was performed under the following conditions: lead nitrate concentration of 100 ppm, lead nitrate volume of 500 mL and photocatalyst weight of 0.4 g. The results reveal that the photocatalytic activity increased from 6 to 99 % with an increase in the wt % of sulfur from 0 to 1.5 wt %. However, further increasing the wt % of sulfur above 1.5 wt % has no significant effect on photocatalytic activity.

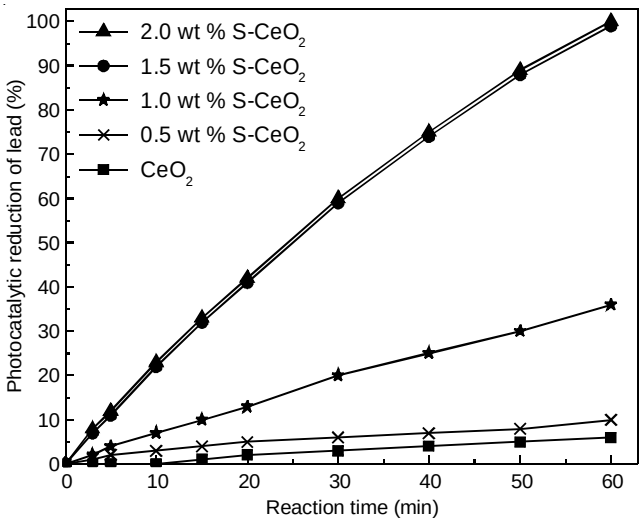

Fug. 6. Effect of the wt % of sulfur on the photocatalytic activity of CeO_2 nanocomposites for the reduction of lead

Fig. 7 shows the effect of loading the 1.5 wt % S-CeO_2 sample on the photocatalytic reduction of lead solution under visible light irradiation. The experiment was performed under the following conditions: lead nitrate concentration of 100 ppm, lead nitrate volume of 1000 mL and a 1.5 wt % S-CeO_2 nanocomposites photocatalyst. The results reveal that photocatalytic performance, in terms of %, after 60 min was increased from 80 to 100 % with an increase in the weight of the photocatalyst from 0.8 to 0.8 g/L. The reaction time required to complete the reduction of lead was decreased to 60, 50 and 30 min as the weight of the photocatalyst was increased to 0.8, 1.2 and 1.6 g/L, respectively. However, the reaction time required to complete the reduction of lead was increased again to 40 min with an increase in the weight of the photocatalyst above 1.6 g/L; that is, the optimum weight of the photocatalyst is 1.6 g/L.

Fig. 8 shows the effect of the initial lead nitrate solution concentration on the photocatalytic reduction of lead solution under visible light irradiation, which was studied by varying the initial lead nitrate solution concentration from 25 to 150 ppm in the presence of 1.5 wt % S-CeO_2 photocatalyst. The results demonstrate that the photocatalytic activity remained nearly unchanged with an increase in the initial lead nitrate solution concentration from 25 to 100 ppm after the 30 min of reaction time required to complete the reduction of lead. However, for initial lead solution concentrations above 100 ppm, the reaction time required to complete the reduction of lead was increased to 40 and 60 min by increasing lead solution concentration to 125 ppm and 150 ppm, respectively. The

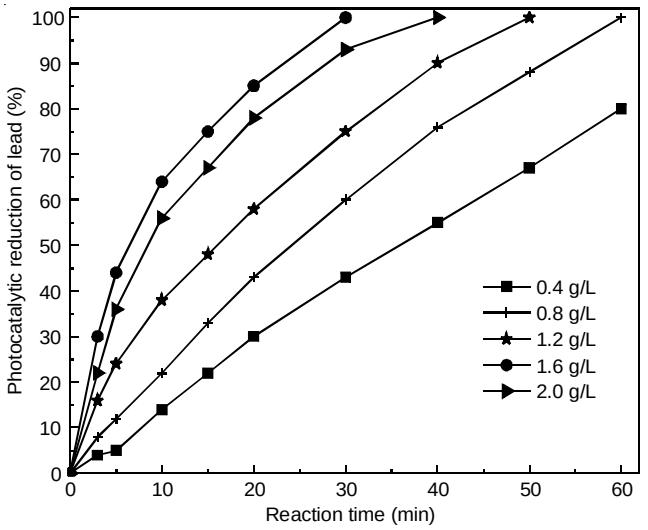

Fig. 7. Effect of loading of the 1.5 wt % S-CeO_2 sample on the photocatalytic reduction of lead

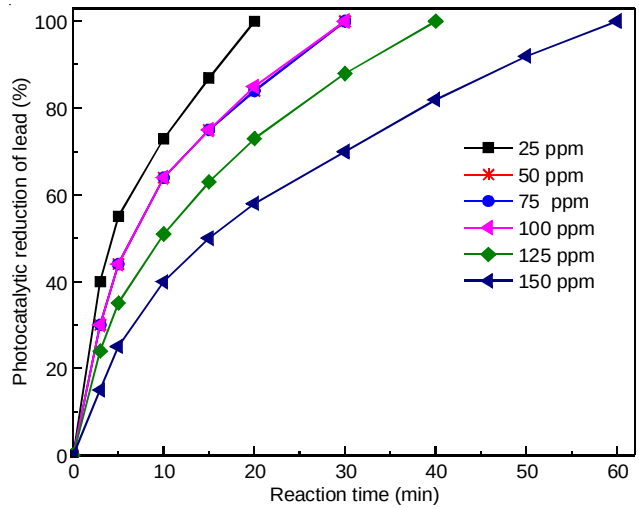

Fig. 8. Effect of the initial lead concentration on the photocatalytic reduction of lead solution

photocatalytic activity depends on the hydroxyl free radicals reaching the surface of the catalyst and then reacting with the cyanide solution. Therefore, increasing the initial lead solution concentration increases the probability of a reaction between the free radicals and the lead solution, thereby increasing the photocatalytic activity. A further increase in the initial lead solution concentration decreases the photocatalytic activity because the active sites of the photocatalyst are blocked by the lead solution, which prevents visible light from penetrating the surface of active sites.

Testing the photocatalyst for multiple cycles is an important factor for commercial use of the photocatalyst. Fig. 9 shows the recycled 1.5 wt % S-CeO_2 photocatalyst for five times. The results demonstrate that the photocatalytic activity remained unchanged after recycling five times.

Conclusion

In summary, a S-CeO_2 nanocomposite photocatalyst was successfully synthesized and proven to be a promising catalyst due to its high efficiency in reducing the pollutant lead under visible light. The band gap of the CeO_2 photocatalyst can be

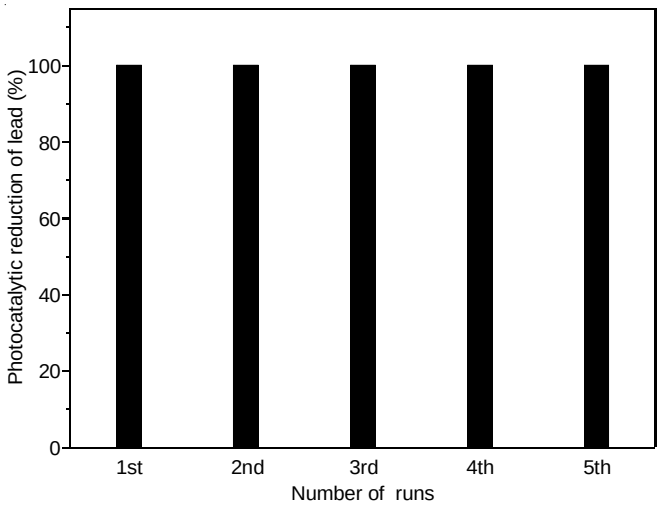

Fig. 9. Recycling and reuse of the 1.5 wt % S-CeO_2 nanocomposite for the photocatalytic reduction of lead

controlled by controlling the weight percent of sulfur that is deposited onto the surface of the photocatalyst. The results of photocatalytic studies reveal that the highest photocatalytic activity and stability were obtained for the 1.5 wt % S-CeO_2 nanocomposite photocatalyst, which can be used to reduced 100 % of lead after 30 min.

REFERENCES

1. ATSDR, Priority List of Hazardous Substances, Atlanta (2013).
2. EPA, National Primary Drinking Water Regulations (2013).
3. European Commission, Scientific Committee on Health and Environmental Risks (2011).
4. R. Shawabkeh, *Process Saf. Environ. Prot.*, **87**, 261 (2009).
5. R.A. Shawabkeh and E.S.M. Abu-Nameh, *Colloid J.*, **69**, 355 (2007).
6. R.F.P. Pereira, A.J.M. Valente and H.D. Burrows, *J. Colloid Interf. Sci.*, **414**, 66 (2014).
7. D.M. Burke, M.A. Morris and J.D. Holmes, *Sep. Purif. Technol.*, **104**, 150 (2013).
8. Z. Badani, H. Ait-Amar and A. Si-Salah, *Desalination*, **206**, 295 (2007).
9. J.-W. Zhang, H. Fang, J.-W. Wang, L.-Y. Hao, X. Xu and C.-S. Chen, *J. Membr. Sci.*, **450**, 197 (2014).
10. H.T. Chang, N.M. Wu and F. Zhu, *Water Res.*, **34**, 407 (2000).
11. L. Chen, M.E. Graham, G. Li, D.R. Gentner, N.M. Dimitrijevic and K.A. Gray, *Thin Solid Films*, **517**, 5641 (2009).
12. D. Sun, J. Liu, J. Li, Z. Feng, L. He, B. Zhao, T. Wang, R. Li, S. Yin and T. Sato, *Mater. Res. Bull.*, **53**, 163 (2014).
13. C. Yu, F. Cao, G. Li, R. Wei, J.C. Yu, R. Jin, Q. Fan and C. Wang, *Sep. Purif. Technol.*, **120**, 110 (2013).
14. S.A.K. Leghari, S. Sajjad, F. Chen and J. Zhang, *Chem. Eng. J.*, **166**, 906 (2011).
15. L. Yao, Y.C. Zhang, J. Li and Y. Chen, *Sep. Purif. Technol.*, **122**, 1 (2014).
16. Y. Zhao, Y. Zhang, J. Li and Y. Chen, *Sep. Purif. Technol.*, **129**, 90 (2014).
17. Q. Fu, H. Saltsburg and M. Flytzani-Stephanopoulos, *Science*, **301**, 935 (2003).
18. E.P. Murray, T. Tsai and S.A. Barnett, *Nature*, **400**, 19 (1999).
19. A. Corma, P. Atienzar, H. Garcia and J.Y. Chane-Ching, *Nat. Mater.*, **3**, 394 (2004).
20. A.H. Morshed, M.E. Moussa, S.M. Bedair, R. Leonard, S.X. Liu and N. Elmasry, *Appl. Phys. Lett.*, **70**, 1647 (1997).
21. S. Tsunekawa, T. Fukuda and A. Kasuya, *J. Appl. Phys.*, **87**, 1318 (2000).
22. D. Terribile, A. Trovarelli, J. Llorca, C. de Leitenburg and G. Dolcetti, *J. Catal.*, **178**, 299 (1998).
23. D.M. Lyons, K.M. Ryan and M.A. Morris, *J. Mater. Chem.*, **12**, 1207 (2002).
24. C. Ho, J.C. Yu, T. Kwong, A.C. Mak and S. Lai, *Chem. Mater.*, **17**, 4514 (2005).
25. H.I. Chen and H.Y. Chang, *Ceram. Int.*, **31**, 795 (2005).
26. A. Bumajdad, M.I. Zaki, J. Eastoe and L. Pasupulety, *Langmuir*, **20**, 11223 (2004).
27. R.M. Mohamed and E.S. Aazam, *Int. J. Photoenergy*, **Article ID 928760** (2012).
28. R.M. Mohamed and I.A. Mkhalid, *J. Alloys Comp*, **501**, 301 (2010).